Prospective Radiologic-Pathologic Correlation of macroscopic volume and microscopic extension of nonsolid lung nodules on Thin-section CT Images for sublobar resection and stereotactic radiotherapy planning

Arnaud Beddok , Marie-Laure Chabi-Charvillat , Titouan Kennel , Julien de Wolf , Ciprian Pricopi , Perrine Crequit , Nicolas Girard , Joelle Otz , Alexandre Vallée , Elisabeth Longchampt , Edouard Sage , Matthieu Glorion

PII: S1525-7304(22)00243-1
DOI: https://doi.org/10.1016/j.cllc.2022.11.001
Reference: CLLC 1546

To appear in: *Clinical Lung Cancer*

Received date: Jul 14, 2022
Revised date: Nov 1, 2022
Accepted date: Nov 2, 2022

Please cite this article as: Arnaud Beddok , Marie-Laure Chabi-Charvillat , Titouan Kennel , Julien de Wolf , Ciprian Pricopi , Perrine Crequit , Nicolas Girard , Joelle Otz , Alexandre Vallée , Elisabeth Longchampt , Edouard Sage , Matthieu Glorion , Prospective Radiologic-Pathologic Correlation of macroscopic volume and microscopic extension of nonsolid lung nodules on Thin-section CT Images for sublobar resection and stereotactic radiotherapy planning, *Clinical Lung Cancer* (2022), doi: https://doi.org/10.1016/j.cllc.2022.11.001

Highlights

- Segmentectomy and SBRT are increasingly used for the treatment of nonsolid nodules.
- It is often difficult to correctly assess the limits and the size of nonsolid nodules.
- CT did not underestimate the macroscopic size and microscopic extension of the NSN.

Prospective Radiologic-Pathologic Correlation of macroscopic volume and microscopic extension of nonsolid lung nodules on Thin-section CT Images for sublobar resection and stereotactic radiotherapy planning

Arnaud Beddok[1,2] MD MSc, Marie-Laure Chabi-Charvillat[3] MD, Titouan Kennel[4] MSc, Julien de Wolf[5] MD, Ciprian Pricopi[5] MD, Perrine Crequit[4] MD PhD, Nicolas Girard[7] MD PhD, Joelle Otz[8] MD, Alexandre Vallée[4] MD PhD, Elisabeth Longchampt[9] MD, Edouard Sage[5] MD PhD, Matthieu Glorion[5] MD, MSc

[1]Institut Curie, PSL Research University, Radiation Oncology Department, Proton Therapy Centre, Centre Universitaire, 91898 Orsay, France

[2]Institut Curie, PSL Research University, University Paris Saclay, Inserm LITO, 91898 Orsay, France

[3]Department of Radiology. Hôpital Foch. Suresnes. France

[4]Department of Epidemiology-Data-Biostatistics, Delegation of Clinical Research and Innovation (DRCI), Foch hospital, Suresnes, 92150, France

[5]Department of Thoracic Surgery. Hôpital Foch. Suresnes. France

[6]Department of Thoracic Oncology, Hôpital Foch. Suresnes. France

[7]Department of Thoracic Oncology, Institut Curie, France

[8]Institut Curie, Radiation Oncology Department, Saint-Cloud, France

[9]Department of Pathology. Hôpital Foch. Suresnes. France

[*]Corresponding author: Arnaud Beddok, Department of Radiation Oncology, 25 rue dôUlm 75005 Paris; +33144324504; a.beddok@gmail.com

ABSTRACT

Introduction: The objective of this study was to determine whether computed tomography (CT) could be a useful tool for nonsolid lung nodule (NSN) treatment planning, surgery or

stereotactic body radiation therapy (SBRT), by assessing the macroscopic and microscopic extension of these nodules.

Methods: The study prospectively included 23 patients undergoing anatomic resection at the Foch Hospital in 2020/2021 for NSN with a ground-glass component of more than 50%. Firstly, for each patient, both the macroscopic dimensions of the NSN were assessed on CT and during pathologic analysis. Secondly, the microscopic extension was assessed during pathologic examination. Wilcoxon sign rank tests were used to compare these dimensions. Spearman correlation test and Bland-Altman analysis were used to evaluate the agreement between radiological and pathologic measurements.

Results: On CT, the median largest diameter and volume of NSN were 21 mm and 3780 cc, while on pathologic analysis, they were 15 mm and 1800 cc, respectively. Therefore, the largest diameter and volume of the NSN were significantly higher on CT than on pathological analysis. For microscopic extension, the median largest diameter and volume of NSN were 17 mm and 2040 cc, respectively. No significant difference was observed between the macroscopic size and the microscopic extension assessed during pathologic analysis. Moreover, correlation analysis and Bland-Altman plots showed that radiological and pathologic measurements could provide equivalent precision.

Conclusion: Our study showed that CT did not underestimate the macroscopic size and microscopic extension of NSN and confirmed that CT can be used for NSN treatment planning.

Keywords

Ground-Glass Opacity, Pulmonary Surgical Procedures; Radiosurgery; Computed Tomography, Anatomical Pathology

1. INTRODUCTION

Lung cancer is one of the most frequent cancers in the world with an incidence of 2 million new cases diagnosed in 2020 [1]. Approximately 20% of lung adenocarcinomas manifest on computed tomography (CT) as nonsolid nodules (NSN) [2]. NSN are also called ground-glass opacities (GGOs) or ground-glass nodules (GGNs) [3]. These NSN correspond to focal areas of slightly increased attenuation on CT through which normal lung parenchyma structures, airways, and vessels are visually preserved. They are radiologically divided into two

categories: pure GGOs that contain no solid component and part-solid GGOs that contain both a pure GGO region and a consolidated region [4]. Several guidelines exist for the management of these NSN [5,6] . Biopsy or surgery is often recommended only for NSN that develop a solid component and/or become larger than 6 mm. Unlike solid tumors whose borders are clearly visible on CT images, for NSN the borders are blurred, and it is often difficult to correctly assess the limits and the size of these lesions. Therefore, the real macroscopic volume measured on specimen could be taller or bigger than the volume estimated with CT. Moreover, many studies have demonstrated a correlation between radiological parameters of NSN (size, volume, density, and roundness) and histologic features of invasiveness [7ï10]. However, to our knowledge, no study has so far evaluated the microscopic extension of NSN. Knowledge of the actual macroscopic size and microscopic extension of NSN is essential in the context of new therapeutic approaches for both minimally invasive surgery and stereotactic body radiation therapy (SBRT). The objective of this study was to determine whether CT could be a useful tool for NSN treatment planning (surgery or SBRT) by assessing the macroscopic size and microscopic extension of these nodules. In this perspective, we first compared the dimensions of the NSN observed on a preoperative CT (called radiological gross tumor volume (GTV) = radiological GTV) and those measured at the time of the pathologic examination (pathologic GTV), and second, we measured the microscopic extension of these NSNs.

2. MATERIAL AND METHODS

2.1. Population and treatment details

The study prospectively included patients aged >18 years undergoing anatomic resection (pulmonary segmentectomy or lobectomy) at the Foch Hospital between 05/02/20 and 31/03/21 for an NSN with a ground-glass component of more than 50%. Prior written and informed consent was obtained from all patients and the study was approved by the ethics review board of Foch Hospital (IRB 00012437). The indication for surgery was decided during a thoracic oncology multidisciplinary staff meeting when the size of the NSN increased significantly at 6-month intervals or when a solid component appeared over time, without necessarily requiring a preoperative histologic diagnosis by biopsy. Several studies and the latest I-ELCAP report have indeed proposed in a context of a very small solid component part to consider the overall size of NSN[11ï13]. A maximum delay of one month between CT evaluation and surgery should not be exceeded. Surgery consisted of lobectomy

or segmentectomy by minimally invasive approaches such as video-assisted thoracoscopic surgery (VATS) or robotic assisted thoracoscopic surgery (RATS).

2.2. Radiological analysis assessment

All chest CT scanner were performed over the entire chest during an inspiratory breath-hold in the supine position. Contiguous 0.6 mm thick axial images were routinely reconstructed with high-frequency and standard reconstruction algorithms. High-frequency reconstructions (or lung reconstructions) were used for the detection of the nodules and for the measurements of the entire lesion. Low-frequency (or mediastinal, soft issue, standard) reconstructions were only used to detect and measure the solid part of the lesion in case of part-solid nodule. All patients had a non-injected CT without contrast enhancement and 11/23 had an additional CT scan with contrast enhancement. Contrast material injection was used in some patients to improve vascular structures and mediastinum analysis before surgery. All analyses were performed only on the CT without contrast enhancement. One chest radiologist (M.L.C) with 11 years of experience reviewed CT examinations. For each patient, the largest diameter of the entire lesion was measured first, followed by the diameters of the two orthogonal axes. Those three diameters allowed us to define the radiological GTV (**Figure 1 A-B**). The same measurements were performed for the solid part of the lesion, on the mediastinal window, to confirm that the ground glass component represented more than 50% of the entire lesion.

2.3. Pathologic analysis

The pathologic diagnoses were performed by one expert pathologist (E.L.) who was unaware of the thin section CT findings. Lobectomy specimens were formalin-fixed, by inflating with 10% formalin using a 20ml syringe placed in the bronchus, until specimens were fully expanded, and the pleura was unfolded. The formalin-filled specimens were then placed in formalin for a minimum fixation time of 24 hours. The specimens were then grossed by cutting 5 mm - thick slices perpendicular to the pleural surface. The pathologic GTV was obtained by measuring the tumor in its three dimensions using a graduated ruler. Briefly, length and width were measured grossly on the slice containing the largest tumor surface. Depth was evaluated by pinching the slices with palpable tumor and measuring the space between the thumb and index using a graduated ruler (**Figure 1 C-D**). Tumor slices were then paraffin-embedded, sectioned and stained with hematoxylin-eosin-saffron (HES). Microscopic tumor size was assessed using the tumor slice containing the largest tumor surface (**Figure 1 E**). Length and width were measured microscopically using an intraocular

micrometer. Width corresponded to that of the gross measurement. Besides this, as recommended in the 8th AJCC TNM edition, a maximal dimension cutoff value of 0.5 cm for pathologic invasiveness was used to differentiate invasive adenocarcinoma (IVA) from adenocarcinoma in situ (AIS) and minimally invasive adenocarcinoma (MIA) [14]. The diagnoses were determined using the multidisciplinary adenocarcinoma criteria: MIA was defined as nodules < 3 cm with predominantly lepidic growth and an invasive component size Ò 0.5 cm. IVA was defined as nodules with either an invasive component size > 0.5 cm or the following conditions: (1) histologic subtypes other than a lepidic pattern (i.e., acinar, papillary, micropapillary, and/or solid); (2) myofibroblastic stroma associated with invasive tumor cells; or (3) lymphatic invasion and/or blood vessel invasion and/or pleural invasion and/or necrosis. The final histologic diagnosis was classified as AIS, MIA, and IVA (lepidic adenocarcinoma [IVA-lepidic], acinar adenocarcinoma [IVA-acinar], and papillary adenocarcinoma [IVA-papillary]).

2.4. **Statistical analysis**

The number of subjects to be included was *a priori* calculated to determine if a significant difference existed between the radiological and the pathologic GTV (mean difference of 9, common standard deviation of 6, power of 90%: a minimum of 22 patients was needed). Statistical analysis was performed using descriptive evaluation with the median and the interquartile) for continuous variables, and frequency and percentage for categorical variables. Wilcoxon sign rank tests were used to compare the radiological GTV, the pathologic GTV and the microscopic extension. Moreover, Spearman rank correlation coefficient (Ɉ) was used to examine the relationship between the radiological GTV and pathologic GTV and between pathologic GTV and microscopic extension. The agreement between radiological and pathologic measurements was finally assessed using the Bland-Altman method [15]. As non-gaussian distributions were observed, non-parametric methods were used for Bland-Altman analysis [16]. Therefore, the median was employed instead of the mean, and the 2.5th and 97.5th percentiles were employed instead of the +/- 1.96SD limits. All tests were bilateral with a 5% degree of significance. Statistical analysis was performed with the SAS 9.4 software.

3. RESULTS

3.1. Population

Twenty-three patients were included in this study. The patients were mostly female, 64-years-old, with for the majority (65%) history of smoking (**Table 1**). The ground-glass component

was significantly lower than 50% for each patient. For 87% of the patients (20/23), the diagnosis was not biopsy proven, the treatment decision was only made on CT progression criteria: the NSN initially measured larger than 6 mm, and a significant increase in nodule size had occurred on two successive CT scans 6 months apart[5]. It should be noted that 18F-FDG PET was performed for the majority of the 23 patients (82.6%) with SUV_{max} near 0. Lobectomy was performed for half of the patients. The majority of the 23 patients (82.6%) had IVA (**Table 2**). After a median follow-up of 19 months (IQR:16-23months), all patients were alive without local or metastatic recurrence.

3.2. Comparison of macroscopic NSNs dimensions: radiological and pathologic GTV

On CT, the measurements of the largest diameter in the coronal, axial and sagittal planes were (median, IQR): 21 mm (15 ï 31), 16 mm (8 ï 22), and 15 mm (13 ï 26), respectively. The volume of the NSNs calculated from these measurements (radiological GTV), as the product of the three largest diameters, was (median, IQR): 3780 cc (1820 ï 16368). During pathologic analysis, the measurements of the largest diameter in the three planes were (median, IQR): 15 mm (11 - 30), 12 mm (10 ï 22) and 10 mm (10 ï 15), respectively. The volume of the NSNs calculated from these measurements (pathologic GTV), as the product of the three largest diameters, was (median, IQR): 1800 cc (1000 ï 6750). The largest diameter and the volume of NSN measured on CT were significantly higher than the largest diameter and the volume of NSN measured during pathologic analysis ($p < 0.01$) (**Table 3**).

3.3. Comparison between macroscopic and microscopic pathologic sizes

For ME, the measures of the largest diameter in the three planes were (median, IQR) 17 mm (10 ï 28), 12 mm (9 ï 20) and 10 mm (10 ï 19), respectively. The volume of the NSNs calculated from these measurements, as the product of the three largest diameters, was (median, IQR) 2040 cc (1000 ï 10640). So, there was no significant difference between the pathologic GTV and microscopic extension ($p = 0.986$) (**Table 3**).

3.4. Agreement between CT and pathologic measurements

The Spearman rank correlation test showed that the radiological GTV and the pathologic GTV, and the pathologic GTV and the microscopic extension were significantly correlated: Ɉ=0.828 ($p<0.001$) and Ɉ=0.902 ($p<0.001$), respectively. The Bland-Altman plots showed the variability between radiological GTV and pathologic GTV (**Figures 2A, 2B, 2C**) and between pathologic GTV and microscopic extension (**Figures 2D, 2E, 2F**). The absolute difference

between radiological GTV and pathologic GTV was 5 mm (limits of agreement: -3 to 15 mm). The absolute difference between pathologic GTV and microscopic extension was 0 mm (limits of agreement: -9 to 5 mm). Same kinds of results were observed for relative differences and logarithmic differences (**Figures 2B, 2D** and **2C, 2F**, respectively). Therefore, the results of correlation analysis and Bland-Altman plots showed that radiological GTV with pathologic GTV as pathologic GTV with microscopic extension could provide equivalent precision.

4. DISCUSSION

In the present prospective study, the radiological-pathologic analysis revealed that the macroscopic size of NSN measured on CT (radiological GTV) was higher than the macroscopic size of NSN measured during pathologic analysis (pathologic GTV). A second pathologic analysis did not find any difference between the pathologic GTV and the microscopic extension of NSN.

Several authors have studied the correlation between radiological and pathologic characteristics of NSN. In 2012, Zhang *et al.* have compared in 15 patients the soft tissue component of NSN between CT and pathological analysis, based for CT on HU attenuation [17]. They showed a significant linear correlation between these two measures. In a retrospective study including 423 resected NSN, Li *et al.* (2018) evaluated the clinical and CT imaging differences in patients with invasive adenocarcinoma (IVA) from adenocarcinoma in situ (AIS) and minimally invasive adenocarcinoma (MIA) [7]. They observed in particular that a tumor size > 13.50 mm, mixed ground-glass opacity nodules and a bubble-like sign were more likely to be diagnosed as IVA. Moreover, Yanagawa *et al.* (2018) have reported in a retrospective multicenter study including 378 patients with NSN a correlation between the maximal dimension of the solid portion of NSN in CT and the tumor pathologic invasiveness [10]. They have demonstrated that a solid portion > 0.8 cm on the lung window setting or > 0.6 cm on the mediastinal window setting predicted for pathologic invasiveness > 0.5 cm. Besides this, in a retrospective study including 634 lung adenocarcinomas, Hattori *et al.* (2019) have compared the clinico-pathologic characteristics and the prognosis of patients with solid and NSN [8]. The frequency of histologic invasiveness, pathologic lymphatic or vascular invasion and nodal metastasis in the solid group was significantly more than that of the NSN group. The five-year Overall Survival was also significantly poorer in the solid nodules group compared to NSN group: 91.2% versus 68.9% ($p < 0.001$), respectively. In another retrospective study including 1290 patients with lung adenocarcinoma, *Aokage et al.* have

also found a correlation between the presence of solid portion on CT and the risk of pathologic invasiveness, especially for lung cancer less than 3 cm in invasive diameter [9]. The results of these two studies are consistent with those of Suzuki *et al.'s* study (2012) [18]. In this prospective multicenter study including 811 patients with clinical T1N0M0 peripheral lung cancers, the authors defined noninvasive peripheral lung adenocarcinoma as an adenocarcinoma Ò 2.0 cm with a consolidation Ò 0.25. In the present study, we compared the macroscopic size of NSN measured on CT and in pathologic analysis, and secondly analyzed the microscopic extension of NSN. In the context of new therapeutic modalities in surgery and radiotherapy, these both points remain essential.

Lobectomy is the most commonly used surgical treatment for NSNs [11]. Nevertheless, some studies have shown that more limited surgery, such as sublobar resection, can be performed [19,20]. In the prospective JCOG0804/WJOG4507L study, *Suzuki et al.* reported the outcomes and safety of 333 patients treated with sublobar resection for NSN defined as maximum tumor diameter Ò 2.0 cm or less and with consolidation tumor ratio Ò0.25 [21]. After a median follow-up of 5.5 years, only two patients died of other causes. The 5 year Overall Survival was 99.4% (95%CI 97.5 ï 99.8%). Grade 3 or higher postoperative complications based on Common Terminology Criteria for Adverse Effect v3.0 were observed in 17 patients (5.4%), without any grade 4 or 5. In this setting, one of the important quality criteria is obviously the surgical margin with the intersegmental plane, especially for nodules close to it [22]. In this case, misjudgment of the ME may lead to a bi-segmentectomy or lobectomy instead of a segmentectomy, especially in the context of minimally invasive surgery, in which nodules cannot be palpated by the surgeon. Moreover, with the emergence of surgical planning, the three-dimensional reconstruction based on CT has become the decisive element in the decision-making for the type of resection to schedule [23]. In the present study, the correlation analysis and Bland-Altman plots showed that radiological GTV with pathologic GTV as pathologic GTV with microscopic extension could provide equivalent precision. Limits of agreements were relatively large, especially for the absolute difference between the pathologic GTV and the microscopic extension (-9 to 5 mm). Nevertheless, these limits of agreement seemed to be consistent with clinical practice since they remained even in their extreme value clearly lower than the minimum margin of 20 mm that thoracic surgeons aim to achieve for NSN resection [24].

Besides this, for patients with comorbidities or other reasons for inoperability, presenting with a peripherally located stage I non-small-cell lung cancer (NSCLC), stereotactic body

radiotherapy (SBRT) is a good option, with local control rates of > 90% at 5 years [25ï27]. In a recent study, Onishi *et al.* reported the outcomes of 84 patients with NSN treated with SBRT [28]. After a median follow-up of 33 months, no patient had local failure nor regional lymph node failure. The 3-year rate of distant failure was 2.6%. In another recent study, Mikami *et al*. reported the clinical and radiological outcomes of 126 patients treated for 133 NSN with SBRT [29]. After a median follow-up of 64.3 months, no local or regional recurrence was observed. It is well-known that for solid tumors, there is a ME of 6 to 8 mm around the radiological GTV for squamous cell carcinomas and for adenocarcinomas respectively [30] and this margin is commonly applied in conventional radiotherapy. For NSN treated with SBRT, the margin around the GTV is actually very rarely specified in the above-mentioned studies. Since the present study showed no significant difference between pathologic GTV and microscopic extension, and the Bland-Altman analysis showed that almost all absolute differences between pathologic GTV and microscopic extension were close to zero, the usual practice of not using an additional margin around the GTV seems to be confirmed here. Furthermore, it is usual to add 5 to 10 mm around the GTV to construct the PTV [31], which seems therefore consistent with the observed extreme Bland-Altman limit of agreement. Further dosimetric studies with a larger number of patients would be useful to confirm this point.

For each patient, measurements were performed in the three axes in order to confirm that the ground-glass component was more than 50%. Revel *et al.* demonstrated that detection of the solid part on the mediastinal window improved interobserver agreement on NSN classification and that the presence of a measurable solid component on the mediastinal window was correlated to adenocarcinoma invasiveness with high specificity [32]. Moreover, several methods have been described to calculate the solid and ground glass portion of NSNs. Several teams used the tumor disappearance ratio (TDR) defined as follows [33]: On a HRCT slice, the maximum tumor diameter is measured on lung setting (DL). On mediastinal setting, the ground-glass area disappears leaving only the consolidation area. The remaining consolidation area maximum diameter is measured (DM). TDR is calculated as 1 ï DM/DL. In the *JCOG 0201 study,* the consolidation/tumor ratio was the most specific and sensitive criteria to distinguish between noninvasive and invasive tumor [18]. This criterion was used in our study.

A major issue of our study was initially to choose the method of estimating the dimension of NSNs on the CT, which may be slightly overestimated when compared to the volume

usually automatically calculated. Nevertheless, this measurement method was selected to best reflect the measurement technique used by pathologists after formalin fixation. As described above, it is fairly difficult to perform a precise classification of NSN on an uninflated, typically stained frozen section [34]. To facilitate the examination, a method of reinflation of the alveolar structure by replacing alveolar air with formalin solution was used. Moreover, the height of the pathologic GTV was estimated by pinching the tumor between the thumb and forefinger, which could be sometimes tricky. Hence, our measurement methods had weaknesses, but they were the ones that seemed the least objectionable. Only a prospective study could be answer to both questions. Indeed, these measurements (either on CT, or pathologic) are not currently performed, and all the measurements should be performed with exactly the same method.

Another limitation of the present study is the small number of patients included. However, it should be noted that this was the very first study comparing the radiological and pathologic size of NSN: we had no reference to determine the number of subjects to include. Therefore, we conducted a preliminary study on four patients. Based on this analysis, the mean difference observed between the largest diameter measured on CT and during pathologic analysis was 9 mm, with standard deviation of 6 mm, and to obtain a power of 90%, the minimal number of patients to be included had to be 22. This number of patients allowed us to conduct our prospective study during the last three years despite the COVID pandemic which delayed the rhythm of inclusions. The inclusion of these 23 patients required the creation of a dedicated workflow that would be now difficult to reactivate. We have therefore attempted to be as accurate as possible regarding the method of radiological and pathologic analysis, to allow another team to validate these results on an external cohort of patients.

As a conclusion, our study showed that the CT does not underestimate the true macroscopic size and microscopic extension of the NSN, and confirmed that CT can be used for the treatment planning (surgery or SBRT) for NSN.

Data availability statement: All data generated and analyzed during this study are included in this published article (and its supplementary information files).

Funding: None

Conflict of Interest

None

5. REFERENCES

1. Sung H, Ferlay J, Siegel RL, et al. Global cancer statistics 2020: GLOBOCAN estimates of incidence and mortality worldwide for 36 cancers in 185 countries. *CA: A Cancer Journal for Clinicians*. n/a(n/a). doi:https://doi.org/10.3322/caac.21660

2. Henschke CI, Yankelevitz DF, Mirtcheva R, McGuinness G, McCauley D, Miettinen OS. CT Screening for Lung Cancer: Frequency and Significance of Part-Solid and Nonsolid Nodules. *American Journal of Roentgenology*. 2002;178(5):1053-1057. doi:10.2214/ajr.178.5.1781053

3. Naidich DP, Bankier AA, MacMahon H, et al. Recommendations for the management of subsolid pulmonary nodules detected at CT: a statement from the Fleischner Society. *Radiology*. 2013;266(1):304-317. doi:10.1148/radiol.12120628

4. Pedersen JH, Saghir Z, Wille MMW, Thomsen LH, Skov BG, Ashraf H. Ground-Glass Opacity Lung Nodules in the Era of Lung Cancer CT Screening: Radiology, Pathology, and Clinical Management. *Oncology (Williston Park, NY)*. 2016;30(3):266-274.

5. MacMahon H, Naidich DP, Goo JM, et al. Guidelines for Management of Incidental Pulmonary Nodules Detected on CT Images: From the Fleischner Society 2017. *Radiology*. 2017;284(1):228-243. doi:10.1148/radiol.2017161659

6. Jaklitsch MT, Jacobson FL, Austin JHM, et al. The American Association for Thoracic Surgery guidelines for lung cancer screening using low-dose computed tomography scans for lung cancer survivors and other high-risk groups. *J Thorac Cardiovasc Surg*. 2012;144(1):33-38. doi:10.1016/j.jtcvs.2012.05.060

7. Li M, Wang Y, Chen Y, Zhang Z. Identification of preoperative prediction factors of tumor subtypes for patients with solitary ground-glass opacity pulmonary nodules. *J Cardiothorac Surg*. 2018;13(1):9. doi:10.1186/s13019-018-0696-7

8. Hattori A, Hirayama S, Matsunaga T, et al. Distinct Clinicopathologic Characteristics and Prognosis Based on the Presence of Ground Glass Opacity Component in Clinical Stage IA Lung Adenocarcinoma. *J Thorac Oncol*. 2019;14(2):265-275. doi:10.1016/j.jtho.2018.09.026

9. Aokage K, Miyoshi T, Ishii G, et al. Influence of Ground Glass Opacity and the Corresponding Pathological Findings on Survival in Patients with Clinical Stage I Non-Small Cell Lung Cancer. *J Thorac Oncol*. 2018;13(4):533-542. doi:10.1016/j.jtho.2017.11.129

10. Yanagawa M, Kusumoto M, Johkoh T, et al. Radiologic-Pathologic Correlation of Solid Portions on Thin-section CT Images in Lung Adenocarcinoma: A Multicenter Study. *Clin Lung Cancer*. 2018;19(3):e303-e312. doi:10.1016/j.cllc.2017.12.005

11. Yankelevitz DF, Yip R, Smith JP, et al. CT Screening for Lung Cancer: Nonsolid Nodules in Baseline and Annual Repeat Rounds. *Radiology*. 2015;277(2):555-564. doi:10.1148/radiol.2015142554

12. Yip R, Wolf A, Tam K, et al. Outcomes of lung cancers manifesting as nonsolid nodules. *Lung Cancer*. 2016;97:35-42. doi:10.1016/j.lungcan.2016.04.005

13. Henschke CI. International Early Lung Cancer Action Program: Screening Protocol. Published 2022. https://www.ielcap.org/sites/default/files/I-ELCAP-protocol.pdf

14. Travis WD, Brambilla E, Noguchi M, et al. International association for the study of lung cancer/american thoracic society/european respiratory society international multidisciplinary classification of lung adenocarcinoma. *J Thorac Oncol*. 2011;6(2):244-285. doi:10.1097/JTO.0b013e318206a221

15. Bland JM, Altman DG. Statistical methods for assessing agreement between two methods of clinical measurement. *Lancet*. 1986;1(8476):307-310.

16. Twomey PJ. How to use difference plots in quantitative method comparison studies. *Ann Clin Biochem*. 2006;43(Pt 2):124-129. doi:10.1258/000456306776021616

17. Zhang L, Yankelevitz DF, Carter D, Henschke CI, Yip R, Reeves AP. Internal growth of nonsolid lung nodules: radiologic-pathologic correlation. *Radiology*. 2012;263(1):279-286. doi:10.1148/radiol.11101372

18. Suzuki K, Koike T, Asakawa T, et al. A prospective radiological study of thin-section computed tomography to predict pathological noninvasiveness in peripheral clinical IA lung cancer (Japan Clinical Oncology Group 0201). *J Thorac Oncol*. 2011;6(4):751-756. doi:10.1097/JTO.0b013e31821038ab

19. Aokage K, Yoshida J, Hishida T, et al. Limited resection for early-stage non-small cell lung cancer as function-preserving radical surgery: a review. *Japanese Journal of Clinical Oncology*. 2017;47(1):7-11. doi:10.1093/jjco/hyw148

20. Cho SK. Surgical Extent for Ground Glass Nodules. *J Chest Surg*. 2021;54(5):338-341. doi:10.5090/jcs.21.029

21. Suzuki K, Watanabe SI, Wakabayashi M, et al. A single-arm study of sublobar resection for ground-glass opacity dominant peripheral lung cancer. *J Thorac Cardiovasc Surg*. 2022;163(1):289-301.e2. doi:10.1016/j.jtcvs.2020.09.146

22. Zuo YZ, Liu C, Liu SW. Pulmonary intersegmental planes: imaging appearance and possible reasons leading to their visualization. *Radiology*. 2013;267(1):267-275. doi:10.1148/radiol.12121114

23. Sarsam M, Glorion M, de Wolf J, et al. The role of three-dimensional reconstructions in understanding the intersegmental plane: an anatomical study of segment 6. *Eur J Cardiothorac Surg*. 2020;58(4):763-767. doi:10.1093/ejcts/ezaa123

24. Sawabata N, Ohta M, Matsumura A, et al. Optimal distance of malignant negative margin in excision of nonsmall cell lung cancer: a multicenter prospective study. *Ann Thorac Surg*. 2004;77(2):415-420. doi:10.1016/S0003-4975(03)01511-X

25. Baumann P, Nyman J, Hoyer M, et al. Outcome in a prospective phase II trial of medically inoperable stage I non-small-cell lung cancer patients treated with stereotactic body radiotherapy. *J Clin Oncol*. 2009;27(20):3290-3296. doi:10.1200/JCO.2008.21.5681

26. Lindberg K, Nyman J, Riesenfeld Källskog V, et al. Long-term results of a prospective phase II trial of medically inoperable stage I NSCLC treated with SBRT - the Nordic experience. *Acta Oncol*. 2015;54(8):1096-1104. doi:10.3109/0284186X.2015.1020966

27. Postmus PE, Kerr KM, Oudkerk M, et al. Early and locally advanced non-small-cell lung cancer (NSCLC): ESMO Clinical Practice Guidelines for diagnosis, treatment and follow-up. *Ann Oncol*. 2017;28(suppl_4):iv1-iv21. doi:10.1093/annonc/mdx222

28. Onishi H, Shioyama Y, Matsumoto Y, et al. Stereotactic body radiotherapy in patients with lung tumors composed of mainly ground-glass opacity. *J Radiat Res*. 2020;61(3):426-430. doi:10.1093/jrr/rraa015

29. Mikami N, Takeda A, Hashimoto A, et al. CT Findings and Treatment Outcomes of Ground-Glass Opacity Predominant Lung Cancer After Stereotactic Body Radiotherapy. *Clin Lung Cancer*. 2022;23(5):428-437. doi:10.1016/j.cllc.2022.03.007

30. Giraud P, Antoine M, Larrouy A, et al. Evaluation of microscopic tumor extension in nonïsmall-cell lung cancer for three-dimensional conformal radiotherapy planning. *International Journal of Radiation Oncology*Biology*Physics*. 2000;48(4):1015-1024. doi:10.1016/S0360-3016(00)00750-1

31. Ball D, Mai GT, Vinod S, et al. Stereotactic ablative radiotherapy versus standard radiotherapy in stage 1 non-small-cell lung cancer (TROG 09.02 CHISEL): a phase 3, open-label, randomised controlled trial. *Lancet Oncol*. 2019;20(4):494-503. doi:10.1016/S1470-2045(18)30896-9

32. Revel MP, Mannes I, Benzakoun J, et al. Subsolid Lung Nodule Classification: A CT Criterion for Improving Interobserver Agreement. *Radiology*. 2018;286(1):316-325. doi:10.1148/radiol.2017170044

33. Yoshida J. Management of the peripheral small ground-glass opacities. *Thorac Surg Clin*. 2007;17(2):191-201, viii. doi:10.1016/j.thorsurg.2007.03.010

34. Mori M, Chiba R, Takahashi T. Atypical adenomatous hyperplasia of the lung and its differentiation from adenocarcinoma. Characterization of atypical cells by morphometry and multivariate cluster analysis. *Cancer*. 1993;72(8):2331-2340. doi:10.1002/1097-0142(19931015)72:8<2331::aid-cncr2820720808>3.0.co;2-e

6. FIGURE CAPTIONS

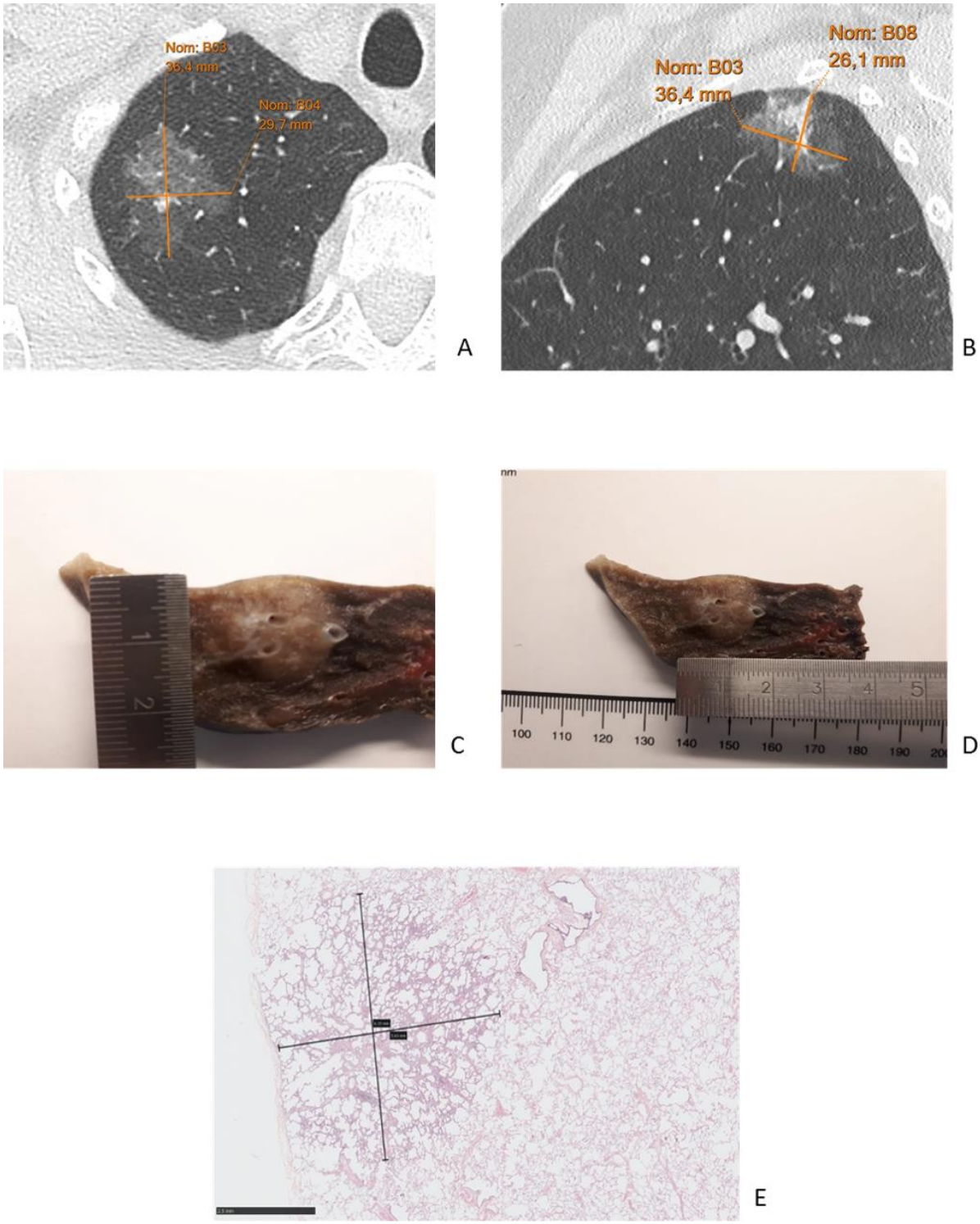

Figure 1: Methods of measurement of nodule size on CT (radiological GTV) and during pathologic analysis (pathologic GTV and microscopic extension (ME))

A, B: For each patient, the largest diameter of the entire lesion was measured first (B03), followed by the diameters of the two orthogonal axes (B04 and B08). These three diameters allowed us to define the radiological volume of the lesion. C, D: During pathologic analysis,

gross tumor size (GTV) was obtained by measuring the tumor using a graduated ruler. Here length (C) and width (D) were measured on the largest tumor surface. E: Microscopic tumor size (CTV) was assessed using an intraocular micrometer on the largest tumor surface, stained with hematoxylin eosin (HE); original magnification x 20.

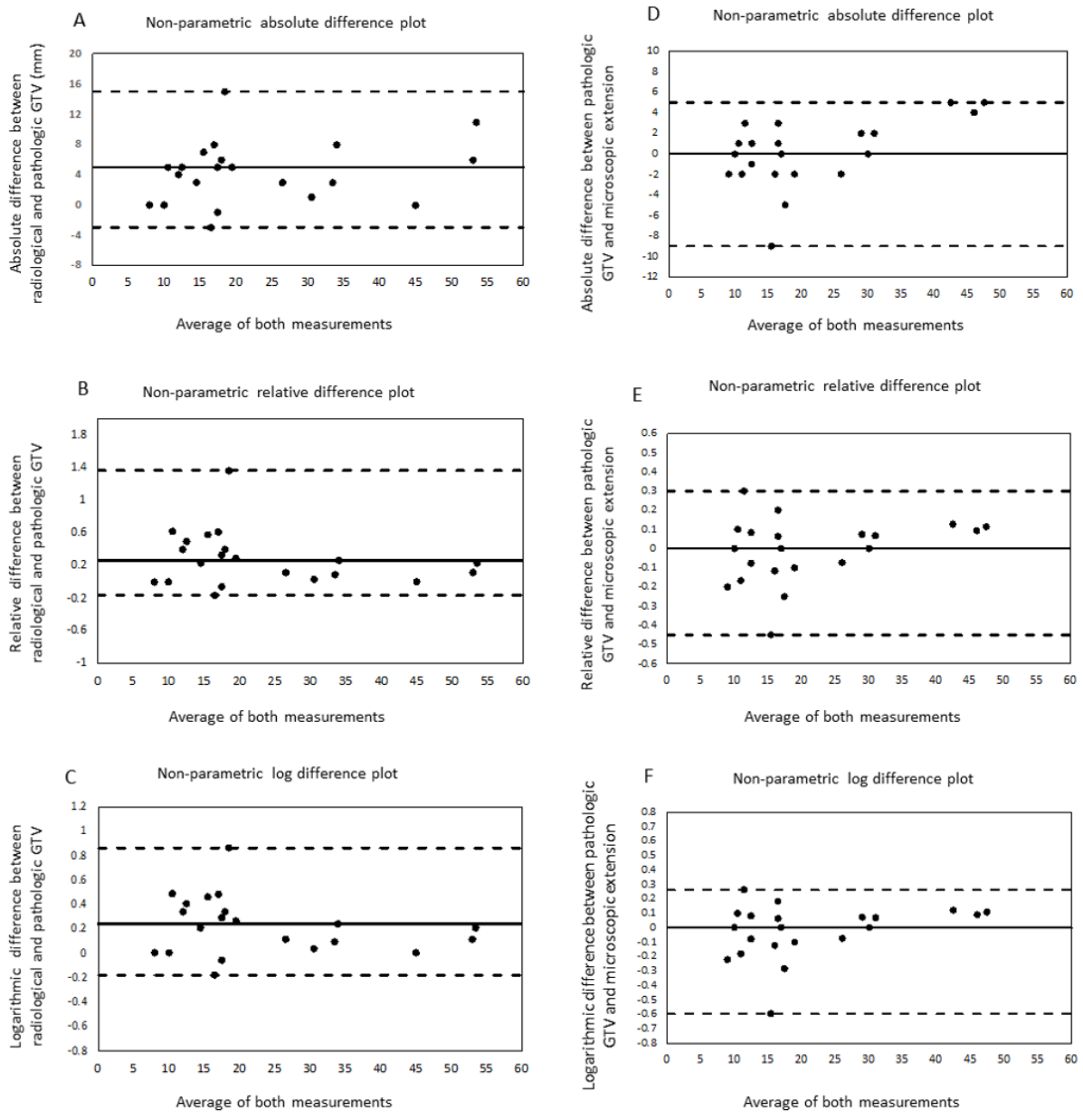

Figure 2: Bland-Altman analysis between radiological GTV and pathologic GTV (A, B, C) and between pathologic GTV and microscopic extension (D, E, F). The figures 2A, 2B and 2C show the absolute, relative and logarithmic differences plots between radiological GTV and pathologic GTV with non-parametrically derived 95% limits of agreement using median, 2.5th percentile and 97.5th percentile, respectively. The absolute, relative and logarithmic differences between radiological GTV and pathologic GTV were 5 mm (limits of agreement: -

3 to 15 mm), 0.267 (limits of agreement: -0.167 to 1.363) and 0.236 (limits of agreement: -0.182 to 0.860), respectively. The figures 2D, 2E and 2F show the absolute, relative and logarithmic differences plots between the pathologic GTV and the microscopic extension with non-parametrically derived 95% limits of agreement using median, 2.5^{th} percentile and 97.5^{th} percentile, respectively. The absolute, relative and logarithmic differences between pathologic GTV and microscopic extension were 0 mm (limits of agreement: -9 to 5 mm), 0 (limits of agreement: - 0.45 to 0.3) and 0 (limits of agreement: - 0.59 to 0.26), respectively. Therefore, the results of correlation analysis and Bland-Altman plots showed that radiological GTV with pathologic GTV as pathologic GTV with microscopic extension could provide equivalent precision.

Table 1: Characteristics of the 23 patients operated for non-solid tumors

Characteristics	N=23	%
Age (median, interquartile)	64 (56 ς 70)	
Gender		
Male	8	34.8
Female	15	65.2
ECOG		
2	1	4.3
1	2	8.7
0	20	87
Smoking status		
Active	7	30.4
Former	8	34.8
Never	8	34.8
Location		
Upper right lobe	7	30.4
Middle lobe	2	8.7
Lower right lobe	6	26.1
Upper left lobe	8	34.8
Diagnostic of NSN		
Biopsy	3	13
Imaging	20	87
Non-solid nodule (NSN)		
Solid part volume (cc, [median, interquartile])	4 (0 ς 144)	
Ground glass opacity (GGO) part volume (cc, [median, interquartile])	3780 (1820 ς 16368)	
Solid/GGO (%, [median, interquartile])	0.07 (0 ς 2.07)	
Delay between scanner and intervention (days, [median, interquartile])	16 (8 ς 22)	
Surgery		
Segmentectomy	12	52
Lobectomy	11	48
Minimal invasive surgery	23	100
VATS	5	21.7
RATS	18	78.3

Abbreviations: RATS = robotic assisted thoracoscopic surgery; VATS = video-assisted thoracoscopic surgery,

Table 2: Pathologic characteristics of the 23 resected lung cancers

Characteristics	N=23	%
Pathological invasiveness		
AIS	1	4.4
MIA	3	13.0
IVA	19	82.6
IVA-L	8	42.2
IVA-A, IVA-P	11	57.8
pT		
pTis	1	4.4
pT1a	5	21.7
pT1b	10	43.4
pT1c	4	17.5
pT2b	3	13.0
Somatic mutations		
CK7	18	78.2
CK20	2	8.7
TTF1	19	82.6
ALK	1	4.3
ROS	8	34.8
EGFR	3	13.0
PDL-1 status		
≥1%	22	95.7
>1-49%	1	4.3
>50%	0	0

Abbreviations: A = acinar; AIS = adenocarcinoma in situ; IVA = invasive adenocarcinoma; MIA = minimally invasive adenocarcinoma; L = lepidic; P = papillary

Table 3: Comparison between the dimensions of non-solid nodules on CT, macroscopic and microscopic pathological analysis

	Larger Diameter (mm, [median, IQR])	**Macroscopic volume (GTV)**			
		Dimension 1 (mm, [median, IQR])	Dimension 2(mm, [median, IQR])	Dimension 3 (mm, [median, IQR])	Volume (cc, [median, IQR])
Radiological GTV	21 (15 ς 31)	21 (15 ς 31)	16 (8 ς 22)	15 (13 ς 26)	3780 (1820

		(Coronal)	(Axial)	(Sagittal)	ς 16368)
Pathologic GTV	15 (11 ς 30)	15 (11 ς 30) (Length)	12 (10 ς 22) (Width)	10 (10 ς 15) (Height)	1800 (1000 ς 6750)
p-value (Radiological GTV vs. Pathologic GTV)	*p<0.001*				*p<0.001*
Microscopic extension	17 (10 ς 28)	17 (10 ς 28)	12 (9 ς 20)	10 (10 ς 19)	2040 (1000 ς 10640)
p-value (Pathologic GTV vs. Microscopic extension)	*p = 0.836*				*p = 0.750*

Abbreviations: Microscopic extension: microscopic extension of the non-solid nodule assessed during pathological analysis; Pathologic GTV: macroscopic tumoral volume assessed during pathologic analysis; Radiological GTV: macroscopic tumoral volume assessed on CT,